Frontiers in Heat and Mass Transfer (FHMT), 18, 33 (2022)
DOI: 10.5098/hmt.18.33

Global Digital Central
ISSN: 2151-8629

Frontiers in Heat and Mass Transfer

Available at www.ThermalFluidsCentral.org

COUPLING ANALYSIS OF ELECTROMAGNETIC AND TEMPERATURE FIELD IN SELF-FORMED LINING ELECTRIC FURNACE

Lei Zhang[a], Fuyong Su[a,*] Zhi Wen[a], Shuming Tao[b]

[a] *School of Energy and Environmental Engineering, University of Science and Technology Beijing, Beijing, 100083, China*
[b] *Baoshan Iron & Steel Co.,Ltd., ShangHai, 201900, China*

ABSTRACT

To study the electric furnace melting process of different process parameters (e.g., current frequency, electric current intensity, the insertion depth of the electrode column, and water wall temperature) for each field quantity change and the impact of electric furnace slag conditioning, the mathematical model of the electromagnetic and temperature fields of the slag tempering process in electric furnace was established, and the numerical simulation was analyzed by the ANSYS finite element software. Research results show that current skin effect appears with the increase in current frequency, while the difference between the two ends and the center of the magnetic induction intensity distribution decreases and the joule heat increases. Increasing the strength of the current intensity can reduce the thickness and height of slagging and increase the molten pool height. With the increase of the insertion depth of the electrode column, the electric current flow area in the slag pool increases, the system of the equivalent resistance increases, the current and the system's extreme temperature decrease, which is conducive to the quenching and tempering process.

Keywords: *electric furnace; process parameters; electromagnetic field; temperature field; skin effect*.

1. INTRODUCTION

The melting process of materials, including heat transfer and the flow and solidification process, in the electric melting furnace is very complex and is accompanied by the comprehensive action of the Joule thermal, electric, and magnetic fields. In addition to these different phenomena and reactions, different process parameters, such as current intensity, electrode insertion depth, and water wall temperature, have a direct impact on the quality of production. In a study of the electric melting furnace, Ren et al. (2018) established the transient mathematical model of the three-electrode electroslag remelting process, clearly demonstrating the coupling of the electromagnetic, flow, and temperature fields in the solidification process, and studied the influence of current and electrode spacing. Tong et al. (2020) taking the electroslag remelting with pipe electrode (ESR-PE) and electroslag remelting with solid electrode (ESR-SE) as the research objects, a two-dimensional steady-state mathematical model of coupled electromagnetic field equation, energy equation, and flow equation was established. The distribution of its current density, Joule heat, flow field, and temperature field was compared and the difference of their molten metal pool was analyzed. Wang et al. (Wang et al. (2017) and Wang et al. (2016)) studied the influence of current on the slag temperature, the melting rate, and the molten pool depth. Yu et al. (2016) analyzed the distribution characteristics of current density, magnetic field intensity, Lorentz force, and Joule thermal density in the process of electroslag remelting at power frequency and studied the influence of current frequency and electrode insertion depth on the electromagnetic field in the process of electroslag remelting.

Many scholars use Fluent software to do simulation research on electric furnace. Miao et al. (2018) used the MHD model in the Fluent software to calculate the resistance values corresponding to different electrode insertion depths, slag quantities, and slag conductivity values under the steady state condition of ESR and predicted the reasonable electrode insertion depths in different, actual ESR processes. Wang et al. (2011) studied the distributions of magnetic field, electromagnetic force, current density, and Joule heat power density in the two-stage series electroslag remelting process. Hugo et al. (2016) studied the influence of the presence of mold current on the pyroheat, flow function, velocity field, and temperature field in a slag pool and demonstrated the necessity of integrating mold current into the model to predict the solidification conditions of remelted materials accurately. Li et al. (2019) used a two-dimensional axisymmetric steady-state mathematical model to compare the distributions of the electromagnetic field intensity, Joule heat, current density, and temperature of traditional ESR and ESR-CCSM models. Liu et al. (2015) studied the characteristics and differences of current density, magnetic field strength, Lorentz force, and Joule heat in lab- and industrial-scale ESR systems; on this basis, the effect of current frequency on the electromagnetic field of ESR systems was studied. Huang et al. (Huang et al. (2018) and Huang et al. (2020)) proposed a transient model that couples magnetohydrodynamic flow, heat transfer, and material transport. By studying the effect of vacuum on oxygen transfer during electroslag remelting, they found that the hot region is located at the top of the slag, and the maximum temperature and depth of the molten pool increase with the applied current.

In the research of electric furnace production characteristics, Geng et al. (2017) studied the effects of three process parameters, namely, electrode filling rate, slag pool depth, and melting rate, on ESR. Karalis et al. (2016) performed two-dimensional steady-state CFD analysis on an industrial arc furnace and analyzed the influence of electrode shape, immersion depth, and Joule heating on the slag properties. Wang et al. (2018) numerically simulated and analyzed the influence of electrode shrinkage on the ESR process of a 430-mm IN718 alloy ingot with a diameter of by using the self-developed ESR process model and specially

* Corresponding author, E-mail address: sfyong@ustb.edu.cn (Fuyong Su)

Global Digital Central
ISSN: 2151-8629

designing different shapes and sizes of shrinkage holes on the electrode. Ren et al. (2019) developed a transient multi-field coupling mathematical model for the three-phase electrode electroslag remelting process based on the finite volume method. By simplifying Maxwell's equations, an electromagnetic field transport equation applicable to the electroslag remelting system was obtained, and the distributions of Lorentz force and Joule heat were calculated. Dong et al. (2016) studied the influence of droplet formation and departure in the electrode head on the temperature distribution in liquid slag and steel molten pool during electroslag remelting. Previous studies on ESR mostly focused on the distributions of field quantities under the coupling of multiple physical fields (Li et al. (2017), Wang Q et al. (2015), Wang X H et al. (2015), Kelkar et al. (2016), Karimi et al. (2018), Du et al. (2017), Zhang and Fang (2020) and Dong et al. (2016)), but no further systematic study has been conducted on the influence of the various process parameters of the electric melting furnace on field quantities.

On the basis of previous research results, this study aimed at a kind of electric furnace without refractory lining, the electric furnace through external water wall cooling after form in internal lining since. This study is based on the basic theory of electromagnetic field and heat transfer, and the influence of the electric furnace melting process is analyzed in detail by using the ANSYS finite element software in view of the electric furnace smelting process of current frequency, current intensity, electrode insertion depth, and water wall temperature.

2. MATHEMATICAL MODEL OF MELTING PROCESS IN ELECTRIC MELTING FURNACE

2.1 The actual electric furnace

The actual electric furnace studied in this paper is shown in Figure 1. The electric furnace uses three electrodes to heat the slag in the furnace.

Fig. 1 The actual electric furnace

2.2 Mathematical model of electromagnetic field

The slag material in the electric melting furnace is studied in this work. The following assumptions are made. First, the conductivity of the slag in the electric melting furnace is regarded as constant and isotropic. Second, the influence of solven on the electromagnetic field is ignored because the quality of the solvent added for tempering in the smelting process is low. The permeability of electrode and slag is equal to that of vacuum. The slag smelting process is in the quasi-steady state, and the influence of molten pool flow on the electromagnetic field is ignored. The electromagnetic induction phenomenon can be described by Maxwell equations, which are expressed as follows:

$$\begin{cases} \nabla \times \boldsymbol{H} = \boldsymbol{J} + \dfrac{\partial \boldsymbol{D}}{\partial t} \\ \nabla \times \boldsymbol{E} = -\dfrac{\partial \boldsymbol{B}}{\partial t} \\ \nabla \times \boldsymbol{D} = \rho \\ \nabla \times \boldsymbol{B} = 0 \end{cases} . \tag{1}$$

The Lorentz law is expressed as follows

$$\boldsymbol{F} = \boldsymbol{J} \times \boldsymbol{B} . \tag{2}$$

Joule's law is denoted as

$$\omega = \boldsymbol{E} \times \boldsymbol{J} , \tag{3}$$

where $\boldsymbol{H}$ is the magnetic field intensity vector, A/m; $\boldsymbol{J}$ is the total current density vector, A/m^2; $\boldsymbol{D}$ is the electric flux density vector, A/m^2; $\boldsymbol{F}$ is the Lorentz force, N; $\boldsymbol{B}$ is the flux density vector, T; $\boldsymbol{E}$ is the electric field intensity vector, V; and w is the heating density, W/m^3.
The boundary condition of the electrode end is

$$H_x = H_y = \frac{\partial H}{\partial z} = 0 \tag{4}$$

The boundary condition of slag and air is

$$H_x = H_y = 0, H_z = \frac{I}{2\pi r} \tag{5}$$

The boundary condition between the slag and the crystal wall is

$$H_x = H_y = \frac{I}{2\sqrt{2}\pi r}, H_z = 0 \tag{6}$$

2.3 Mathematical model of temperature field

According to the temperature field, the following assumptions were made in this study. The thermophysical parameters of molten slag are constant and isotropic. The influence of solven on the temperature field is ignored because the quality of the solvent added for tempering in the smelting process is low. The forced convective heat transfer generated by the flow in the slag pool is considered by increasing the thermal conductivity. The governing equations of temperature field satisfy the conservation equations of mass, momentum, and energy.
(1) Mass conservation equation

$$\frac{\partial \rho}{\partial t} + \frac{\partial (\rho \boldsymbol{u})}{\partial x} + \frac{\partial (\rho \boldsymbol{v})}{\partial y} + \frac{\partial (\rho \boldsymbol{w})}{\partial z} = 0 \tag{7}$$

where ρ is the fluid density, kg/m^3; t is the time, s; and $\boldsymbol{u}$, $\boldsymbol{v}$, and $\boldsymbol{w}$ are the velocity vectors, m/s.
(2) Momentum conservation equation

$$\begin{cases} \dfrac{\partial (\rho \boldsymbol{u})}{\partial t} + div(\rho \boldsymbol{u} U) = -\dfrac{\partial \rho}{\partial x} + \dfrac{\partial \tau_{xx}}{\partial x} + \dfrac{\partial \tau_{yx}}{\partial y} + \dfrac{\partial \tau_{zx}}{\partial z} + \boldsymbol{F}_x \\ \dfrac{\partial (\rho \boldsymbol{v})}{\partial t} + div(\rho \boldsymbol{v} U) = -\dfrac{\partial \rho}{\partial y} + \dfrac{\partial \tau_{xy}}{\partial x} + \dfrac{\partial \tau_{yy}}{\partial y} + \dfrac{\partial \tau_{zy}}{\partial z} + \boldsymbol{F}_y \\ \dfrac{\partial (\rho \boldsymbol{w})}{\partial t} + div(\rho \boldsymbol{w} U) = -\dfrac{\partial \rho}{\partial z} + \dfrac{\partial \tau_{xz}}{\partial x} + \dfrac{\partial \tau_{yz}}{\partial y} + \dfrac{\partial \tau_{zz}}{\partial z} + \boldsymbol{F}_z \end{cases} \tag{8}$$

where P is the pressure on the fluid element, N; $\boldsymbol{\tau}_{xx}$ is the normal stress, N; $\boldsymbol{\tau}_{yx}$ and $\boldsymbol{\tau}_{zx}$ are the tangential stresses, N; and $\boldsymbol{F}_x$, $\boldsymbol{F}_y$, and $\boldsymbol{F}_z$ are the forces on the indistinguishable body, N.
(3) Energy conservation equation

$$\frac{\partial (\rho T)}{\partial t} + div(\rho \boldsymbol{v} T) = div\left(\frac{k}{C_p} gradT \right) + S_T \tag{9}$$

Global Digital Central
ISSN: 2151-8629

where T is the fluid temperature, K; k is the heat transfer coefficient of the fluid, W/(m K); C_p is the specific heat capacity of the fluid, J/(kg K); and S_T is the viscous dissipation term, J.
The boundary conditions of the slag pond surface are as follows

$$Q = Q_c + Q_r = h(T_s - T_a)A \tag{10}$$

where Q_c is the heat of the convective heat transfer, W; Q_r is the heat of the radiation heat transfer, W; h is the comprehensive heat transfer coefficient, W/(m^2 K); T_s is the surface temperature of the slag tank, K; T_a is the surface temperature of the slag tank, K; and A is the area of the radiation surface, m^2.
The heat of the radiation heat transfer is

$$Q_r = \varepsilon\sigma_0(T_s^4 - T_a^4)A \tag{11}$$

where ε is the blackness, 0.8; and σ is the blackbody radiation constant, 5.669 $\times 10^{-8}$ W/(m^2 K).
In practice, the radiative heat transfer is usually equivalent to the convective heat transfer.

$$h = h_c + h_r = h_c + \varepsilon\sigma_0(T_s^2 - T_a^2)(T_s + T_a) \tag{12}$$

where h_c is the convective heat transfer coefficient, W/(m^2 K); and h_r is the equivalent convective heat transfer coefficient of the radiation heat transfer, W/(m^2 K).

2.4 Model and calculation parameters

The geometrical and physical parameters of the three-phase electric furnace system are shown in Table 1.

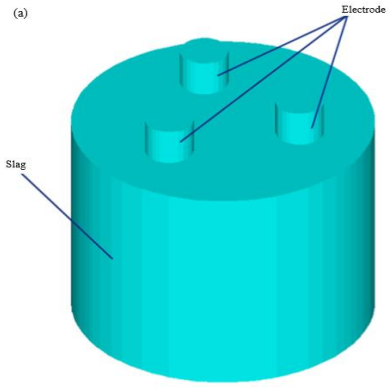

(a) Physical model

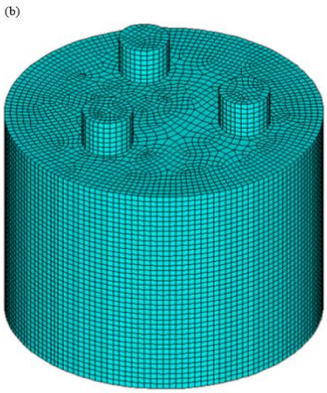

(b) Finite element model

Fig. 2 Model of electric furnace

The physical and finite element models are shown in Fig. 2. Air unit is the default in the calculation process, and the electrode height is set to 0.2 m because the length of the electrode column has no effect on the furnace system. To improve the calculation accuracy, a structured grid is divided between electrode column and slag pool by the mapping and scanning grids. The average grids of the electrode column and the slag tank were set to 0.005 and 0.001 m, respectively. The total number of electric melting furnace system grids is 168591.

Table 1 Parameters used in the model

Name	*Parameter values*
Electrode diameter/m	0.08
Electrode height/m	0.2
Electrode insertion depth/m	0.13
Electric melting furnace diameter /m	0.5
Electric melting furnace height/m	0.4
Voltage/V	50
Electric current /A	4000
Current frequency /Hz	50
Electrode conductivity /(Ω^{-1} m^{-1})	4.34 $\times 10^6$
Slag conductivity /(Ω^{-1} m^{-1})	2 $\times 10^2$
Relative permeability of electrode /(H^{-1} m^{-1})	1
Relative permeability of slag /(H^{-1} m^{-1})	1
Solid phase temperature of slag /℃	1250
Liquid phase temperature of slag /℃	1260
Specific heat capacity of slag /(J kg^{-1} K^{-1})	837
The density of slag /(kg/m^3)	2850
Water wall temperature /℃	50

3. MODEL VALIDATION

Using the established electro-thermal-mass multi-physical coupling mathematical model as basis, scholars have studied the distributions of multiple fields in single- and double-electrode electroslag remelting processes. In this study, the current distribution of Wang and Li (2011) in the double-electrode melting furnace was selected as a reference for establishing the same double-electrode melting furnace physical model, as shown in Fig. 3. The electric current density was for 600 to 1000 kA/m^2, and the magnetic strength was descripted in this literature. The difference in current distribution between the electrode column and the slag pool was explored as shown in Fig. 4. Compared with the literature, the current error in the electrode column established by the two-electrode furnace model is less than 3.5%, and the magnetic induction intensity error in the slag pool is less than 1.8%. Therefore, the mathematical model and research process in this study are reliable.

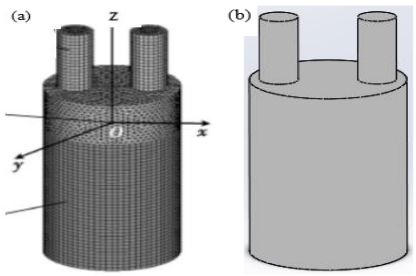

(a) Documentation model;(b) Simulation model

Fig. 3 Physical model

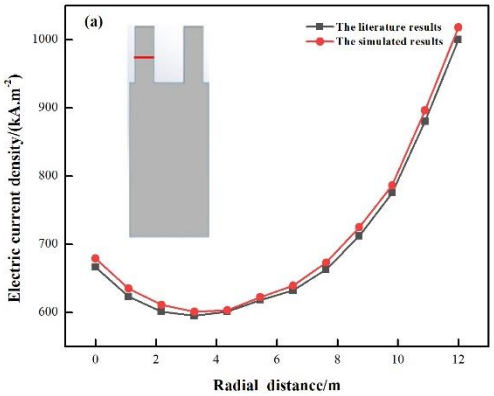

(a) Comparison of the current of the left electrode column

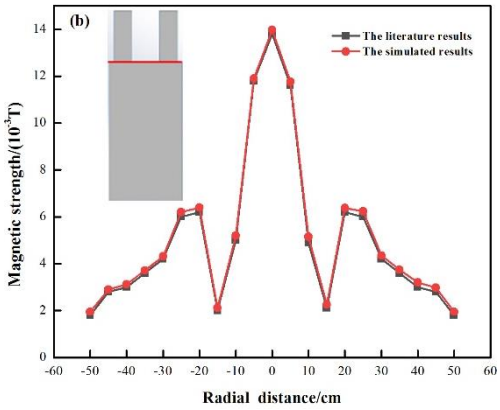

(b) Comparison of magnetic induction intensity of slag pool

Fig. 4 Model verification

4. RESULTS

4.1 Influence of current frequency on melting process of electric melting furnace

When the loading current is 4000 A and the frequencies are 5, 10, 20, 30, 40, and 50 Hz, the current intensity distribution of the electrode column and the slag pool is shown in Fig. 5. In the electrode column, the skin effect is not obvious when the current frequency is below 30 Hz. The difference between the two sides and the center gradually increases with the current frequency. When the current frequency is 50 Hz, the difference between the two sides and the center can reach 98.7 kA/m^2. Given the high resistance in the slag pool, the skin effect will not occur, and the current intensity distribution curve is completely coincident at different frequencies. Given that the current distribution is the basis for the generation of other field quantities, the field quantities in the slag pool will not change at different frequencies.

The magnetic induction intensity and Joule heat distribution in the electrode column at different current frequencies are shown in Fig. 6. The distribution of the magnetic induction intensity in the electrode column is high on both sides and low in the middle, the magnetic induction intensity on the right side is greater than that on the left side, and the magnetic induction intensity exhibits attenuation with the increase in frequency because the skin depth formula is $\delta = (1/\pi f\mu\xi)^{0.5}$. That is, the greater the current frequency is, the smaller the skin depth and the stronger the shielding effect of the electrode column to the magnetic field are. Joule heat exhibits a similar trend as the current in the electrode column. When the current frequency is 5 Hz, the Joule heat distribution in the electrode column remains basically unchanged. The Joule heat difference between the two ends of the electrode column and the center gradually increases with the current frequency. When the current frequency is 50 Hz, the Joule heat difference can reach 46.5 kW/m^2.

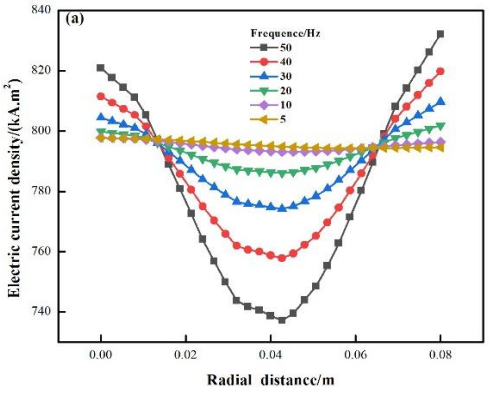

(a) In the electrode column

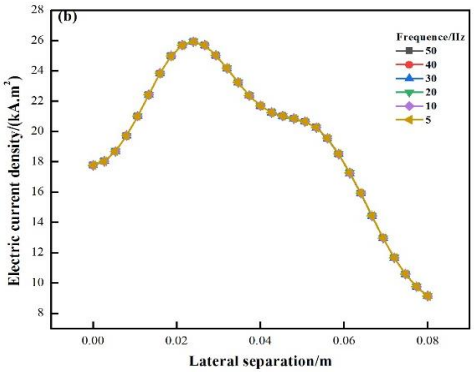

(b) In the slag pool

Fig. 5 Current distribution in electrode column and slag pool at different frequencies

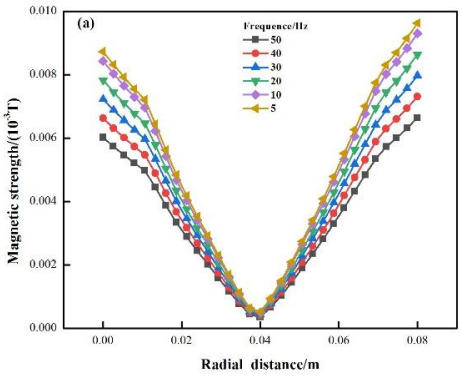

(a) Magnetic strength

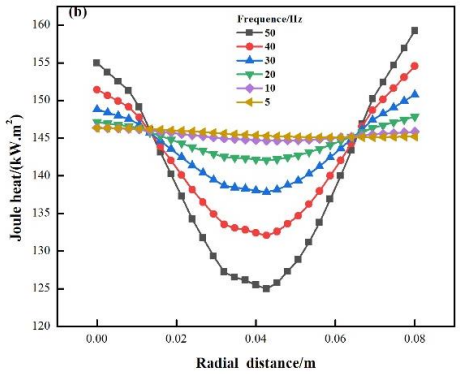

(b) Joule heat

Fig. 6 Magnetic induction intensity and Joule heat distribution in the electrode at different current frequencies

4.2 Effect of current intensity on melting process of electric melting furnace

4.2.1 Electromagnetic fields and temperature fields

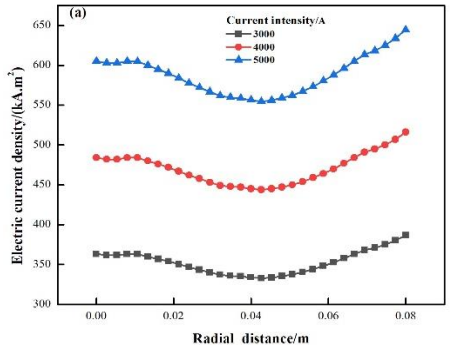

(a) Current density

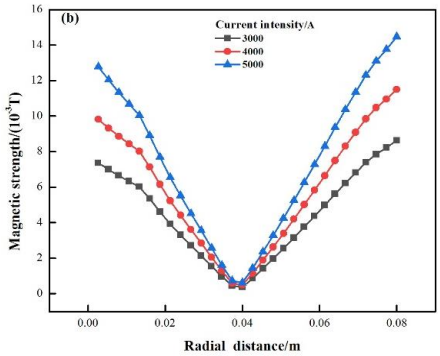

(b) Magnetic strength

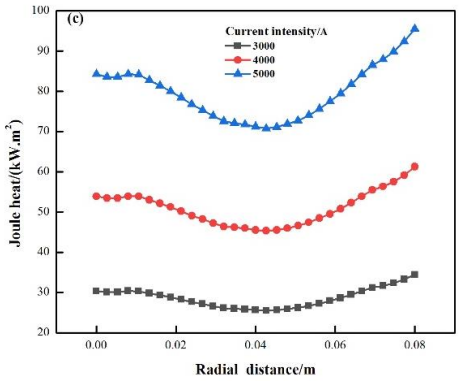

(c) Joule heat

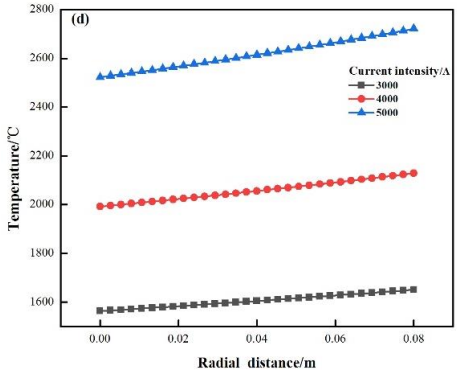

(d) Temperature

Fig. 7 Curves of main field distribution in the electrode at different current intensity

When the electrode column is 0.06 m away from the bottom of the electrode under different current intensities, the distribution curve of the main field quantity is as shown in Fig. 7. The distributions of current, magnetic induction, and Joule heat are higher at both ends and low in the middle, and the right side is slightly higher than the left side. When the current is increased, the pyroheat in the electrode column increases greatly. Thus, the appropriate input current must be used to avoid disrupting the normal operation of the electrode. The temperature in the electrode tends to be low at the left end and high at the right end and is proportional to the radial distance. Given that the thermal resistance is mainly concentrated in the slag pool, the Joule heat generated in the electrode column is far less than that in the slag pool, and the temperature distribution is mainly affected by the Joule heat in the slag pool.

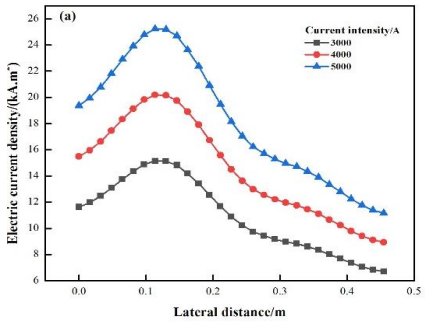

(a) Current density

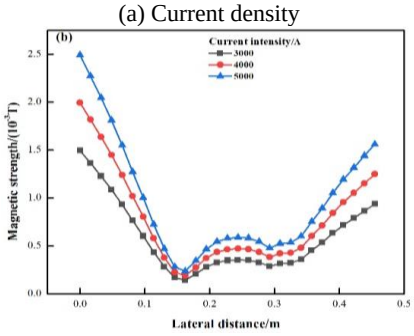

(b) Magnetic strength

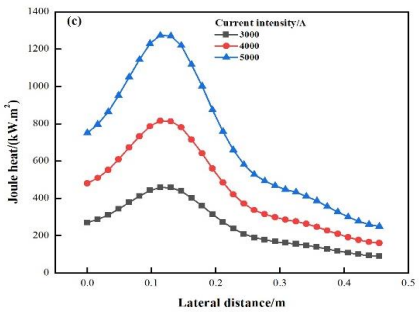

(c) Joule heat

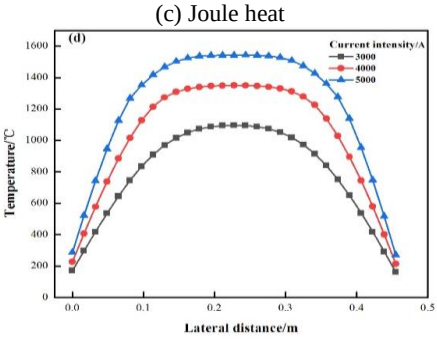

(d) Temperature

Fig. 8 Curves of main field distribution in the slag pool at different current intensity

Fig. 8 shows the distribution curve of the main field quantities in the slag pool at a distance of 0.08 m from the bottom under different current intensities. Fig. 7 indicates that the current distribution of the slag pool tends to be higher on the left than on the right because the input current of the left electrode column is higher than that of the right, and the current distribution increases sharply at the lower end of the electrode column. The magnetic strength is high at both ends and low in the middle, and a steep drop can be observed at the lower end of the electrode column. This effect decreases with the input current. The Joule heat distribution on the left side is higher than that on the right side and increases dramatically below the electrode column. This trend decreases with the increase in slag tank depth. The char heat distribution in the slag tank is greatly affected by the input current and increases sharply with the input current, and the distribution is uneven. In practical operation, attention should be given to prevent the physical properties of slag or the melting electrode from changing due to the high joule heat in the slag bath.

The temperature distribution in the slag pool is high in the middle and low at both ends. The temperature distribution is affected by the joint action of the Joule heat near the electrode and the temperature field of the water wall. The temperature in the slag pool and the high temperature area increase with the intensity of the input current because the increase of the intensity of the current increases the Joule heat near the electrode column. The Joule heat generated by the electrode column at the same position has a stronger influence than that by the water-cooled wall.

4.2.2 Sagging condition of lining

Table 2 shows the influence of current intensity on the heights of the molten pool, the lining slag-forming layer, and the solidification zone. Table 2 indicates that with the increase of the current intensity, the height of the molten pool gradually increases, the slag-forming height decreases, and the height of the solidification zone increases because the temperature in the slag pool increases with the current, and the temperature difference between the slag and the water wall increases, increasing the difficulty of slag solidification. Therefore, in actual production, increasing the current intensity can increase the smelting effect under the condition of ensuring the economic benefit and the normal operation of equipment.

Table 2 Influence of current intensity on heights of molten pool, slag layer, and solidification zone

Current intensity (A)	*Molten pool height* (mm)	*Slagging height* (mm)	*Solidification zone height* (mm)
3000	171.8	226.6	1.6
4000	225.9	172.1	2.0
5000	247.3	150.2	2.5

4.3 Effect of electrode insertion depth on melting process of electric melting furnace

4.3.1 Electromagnetic fields and temperature fields

At 0.06 m from the bottom of the electrode at different electrode insertion depths, the cloud curve of the main field quantity distribution is shown in Fig. 9. Fig. 9 indicates that the current, the magnetic strength, and the Joule heat show a high distribution trend on both sides and a low trend in the middle, and the right side is higher than the left side. The temperature distribution in the electrode column is slightly higher on the right side than on the left side and is proportional to the radial distance. With the increase of the insertion depth of the electrode, the equivalent resistance of the system increases, the current distribution in the electrode column decreases, and the Joule heat and the temperature decrease gradually. The magnetic induction intensity at the center of the electrode remains unchanged, and the difference between the magnetic induction intensities at the surface and the center decreases.

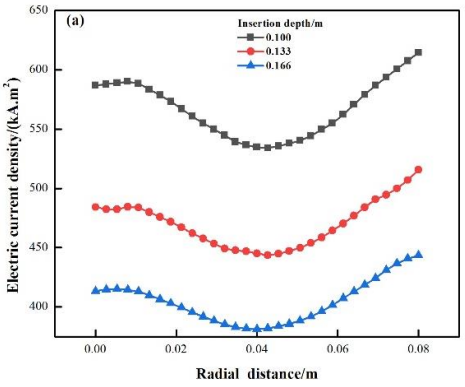

(a) Current density

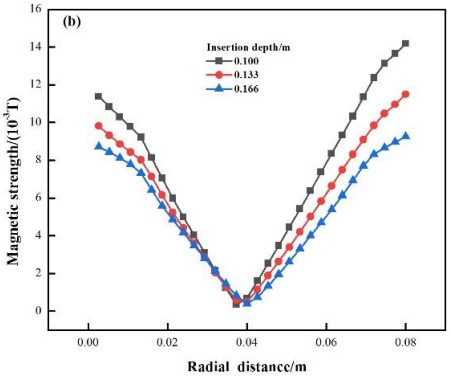

(b) Magnetic induction intensity

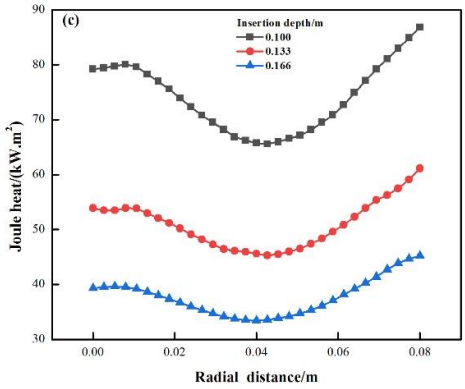

(c) Joule heat

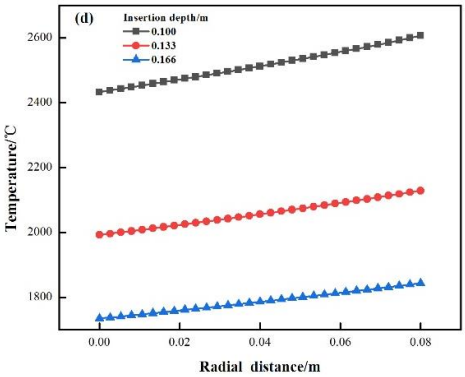

(d) Temperature

Fig. 9 Curves of main field distribution in the electrode at different insertion depth of electrode column

Fig. 10 shows the cloud curve of the main field quantity distribution 0.08 m away from the bottom of the electrode column in the slag pool with different insertion depths of the electrode column.

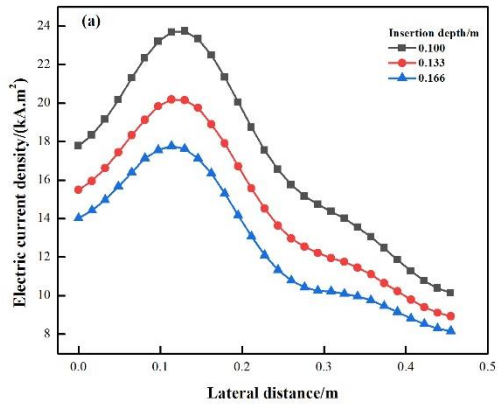

(a) Current density

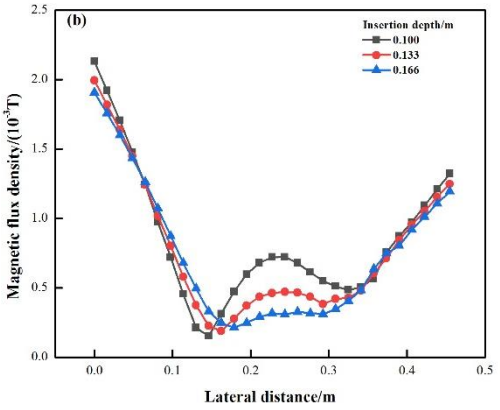

(b) Magnetic induction intensity

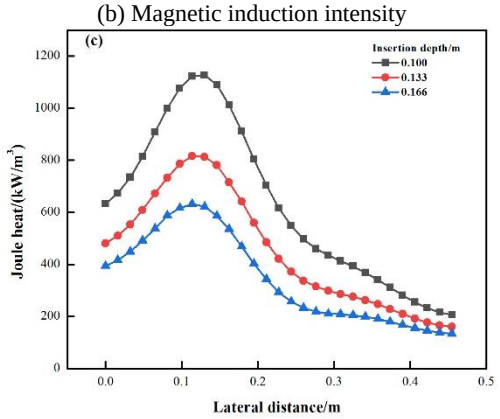

(c) Joule heat

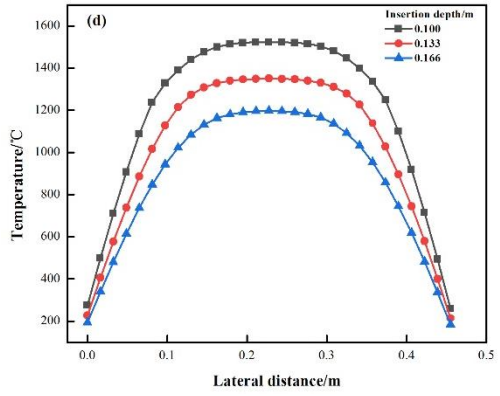

(d) Temperature

Fig. 10 Curves of main field distribution in the slag pool at different insertion depth of electrode column

Fig. 10 indicates that the current distribution in the slag pool is mainly affected by the electrode column because the slag pool resistance is small and has no skin effect. Given that the input current of the electrode column on the left side is larger than the right side, the current distribution on the left side is higher than that on the right side, and the current immediately below the electrode column shows a trend of steep increase. The distribution of magnetic induction intensity is high at both ends and low in the middle, and a steep drop can be observed below the electrode column. The Joule heat distribution is higher on the left side than on the right side and shows a trend of steep increase under the electrode column. The temperature distribution is low at both ends and high in the middle. With the increase of the electrode column insertion depth, the equivalent resistance of the slag pool increases; the current distribution in the slag pool gradually decreases; the magnetic induction intensity, the corresponding Joule heat distribution, and the maximum temperature in the slag pool decrease; but the heat producing area increases, and the temperature in the molten pool becomes more uniform, which is conducive to the process of tempering and tempering. The current, magnetic induction intensity, Joule heat, and temperature decreased by 16.5%, 6.8%, 31.3%, and 10.3%, respectively, with the increase in insertion depth of the electrode column by 0.033 m. Therefore, in actual production, to avoid the possibility of local overburning in the melting process, the insertion depth of the electrode column can be appropriately increased under the condition of ensuring the melting process to maximally reduce the temperature extremum and improve the tempering effect.

4.3.2 Sagging condition of lining

Table 3 shows the influence of the electrode column insertion depth into the molten pool, the lining slag layer, and the solidification zone.

Table 3 Influence of insertion depth of electrode column on heights of molten pool, slag layer, and solidification zone.

Electrode column insertion depth (m)	*Molten pool height* (mm)	*Slagging height* (mm)	*Solidification zone height* (mm)
0.100	213.2	184.0	2.8
0.133	225.9	172.1	2.0
0.166	237.5	160.9	1.6

Table 3 indicates that the depth of the molten pool increases with the electrode insertion depth, the slag height decreases with the increase of the electrode insertion depth, and the height of the solidification zone decreases with the increase of the electrode insertion depth. With the increase of the electrode column insertion depth, the maximum temperature in the slag tank decreases gradually, but the high temperature region increases gradually. Therefore, in actual production, increasing the insertion depth of the electrode column can not only ensure that the central area will not affect the melting due to the high temperature but also increase the melting pool area.

4.4 Influence of water wall temperature on melting process of electric melting furnace

4.4.1 Temperature field

The temperature distributions in the electrode column and the slag pond at different water wall temperatures are shown in Fig. 11. The temperature distributions in the electrode column are low on the left side and high on the right side, while the temperature distributions in the slag pond are low at both ends and high in the middle. The temperature distribution in the slag pool and column electrode gradually increase with the water wall temperature. When the water wall temperature increases 10 ℃, the electrode column temperature increase about 1.5 ℃, slag pool temperature increased 2.3 ℃, because the temperature distribution

in the slag pool is affected by the joule heat near the electrode column and water wall temperature. The temperature has a big effect and rise faster near the water wall, as approach to the center of the electrode column wall, the water wall's effect gradually decreases, and the temperature rise speed slow.

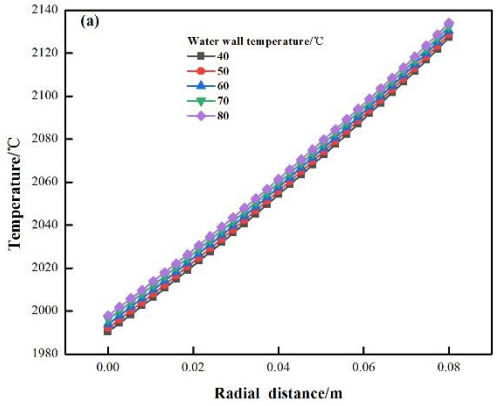

(a) In the electrode column

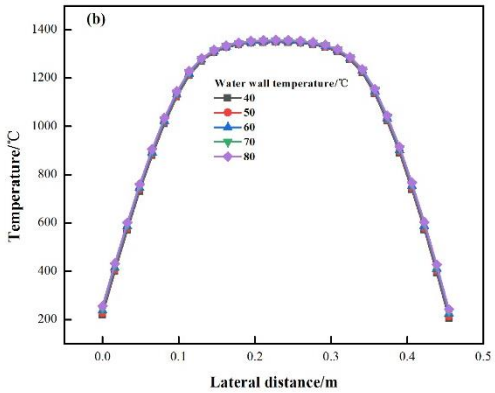

(b) In the slag pool

Fig. 11 Temperature distribution in electrode and slag pool at different water wall temperature

4.4.2 Sagging condition of lining

Table 4 shows the influence of different water wall temperatures on the heights of the molten pool, the lining slag-forming layer, and the solidification zone. Table 4 indicates that the height of the molten pool increases with the water wall temperature, while the heights of the slag-forming layer and the solidification zone decrease with the increase of the water wall temperature. When the water wall temperature increases by 10 ℃, the pool height increases by 0.4 mm, and the slagging height decreases by 0.2 mm. The water wall temperature has little effect on the slagging height.

According to the first law of thermodynamics, the water inflow is calculated through the water wall temperature. If the water is fully heat exchanged in the water wall, then the outlet water temperature is equal to the water wall temperature. When the water wall temperature is 40 ℃, the maximum water inflow is reached. At this time, the inlet water temperature is 20 ℃, the outlet water temperature is 40 ℃, and the heat flow is 394002.8 W/m^2. The maximum water inflow can be calculated as 4.71 kg/s. When the water wall temperature is 80 ℃, the minimum water inflow is reached. At this time, the inlet water temperature is 20 ℃, the outlet water temperature is 80 ℃, and the heat flow is 385815 W/m^2. The minimum water inflow can be calculated as 1.54 kg/s. At this time, the slagging thickness increases by 4.3 mm, and the slagging height increases by 0.8 mm. When the water intake is doubled, the slagging situation changes insignificantly. Therefore, the crystal wall temperature can be kept below 80 ℃ in the actual production.

Table 4 Influence of water wall temperature on heights of molten pool, slag layer, and solidification zone.

Water wall temperature (℃)	*Molten pool height* (mm)	*Slagging height* (mm)	*Solidification zone height* (mm)
40	225.3	172.3	2.4
50	225.9	172.1	2.0
60	226.3	171.8	1.9
70	226.6	171.6	1.8
80	226.8	171.5	1.7

5. CONCLUSIONS

(1) The skin effect of current appears with the increase of the current frequency. The field quantity in the slag pool does not change with the change of the current frequency. The difference between the two ends and the center of the magnetic induction intensity distribution in the electrode column decreases, while the difference between the two ends and the center of the Joule heat distribution increases.

(2) The increase of the input current will lead to the increase of each field quantity, increasing the current can significantly improve the smelting efficiency.

(3) Increasing the electrode column insertion depth will decrease each field quantity. The thickness of the slag layer increases with the insertion depth, preventing the crystallization wall temperature from being extremely high, and the extreme temperature of the system decreases, and the actual melting area increases, which is beneficial to the smelting process.

(4) With the increase of the water wall temperature, the temperature distribution in the slag pool increases gradually, and the volume of the molten pool increases. When the inflow of water is doubled, the slagging situation changes slightly, so the crystal wall temperature can be guaranteed to be lower than the maximum limit temperature (80 ℃) in actual production.

ACKNOWLEDGEMENTS

Financial support was provided by National Key Research and Development Program of China (2018YFB0605904) .

NOMENCLATURE

H	magnetic field intensity vector (A/m)
J	total current density vector (A/m^2)
D	electric flux density vector (A/m^2)
F	Lorentz force (N)
B	flux density vector (T)
E	electric field intensity vector (V)
w	heating density (W/m^3)
P	pressure (N)
t	time (s)
T	fluid temperature (K)
k	heat transfer coefficient of the fluid (W/(m K))
h_c	convective heat transfer coefficient (W/(m^2 K))
Greek Symbols	
ε	total emissivity
ρ	density (kg/m^3)
σ	Stefan-Boltzmann constant (W/m^2 K^4)

Global Digital Central
ISSN: 2151-8629

REFERENCES

Du G, Li J, Wang Z-B, 2017, "Effect of operating conditions on inclusion of die steel during electroslag remelting," *ISIJ International*, ISIJINT-2017-429, http://dx.doi.org/10.2355/isijinternational.ISIJINT-2017-429

Dong Y, Jiang Z, Cao H, Wang X, Cao Y, Hou D, 2016, "A novel single power two circuits electroslag remelting with current carrying mould," *ISIJ International*, 56, 1386-93, http://dx.doi.org/10.2355/isijinternational.ISIJINT-2016-066

Dong Y-W, Jiang Z-H, Fan J-X, Cao Y-L, Hou D, Cao H-B, et al, 2016, "Comprehensive mathematical model for simulating electroslag remelting," *Metallurgical and Materials Transactions B*, 47, 1475-88, http://dx.doi.org/10.1007/s11663-015-0546-0

Huang X, Li B, Liu Z-Q, 2018, "A coupled mathematical model of oxygen transfer in electroslag remelting process," *International Journal of Heat and Mass Transfer*, 120, 458-70, http://dx.doi.org/10.1016/j.ijheatmasstransfer.2017.10.088

Huang X, Li B, Liu Z-Q, 2020, "Numerical study on the effect of vacuum on oxygen transfer in electroslag remelting process, 172, 109069, http://dx.doi.org/10.1016/j.vacuum.2019.109069

Hugo M, Dussoubs B, Jardy A, Escaffre J, Poisson H, 2016, "Influence of the mold current on the electroslag remelting process," *Metallurgical & Materials Transactions B*, 47, 2607-22, http://dx.doi.org/10.1007/s11663-016-0694-x

Geng R, Li J, Shi C, Zhu Q, Zhang J, 2017, "Technology. Numerical simulation of Electroslag Remelting of Cr5 cold roll steel under different process parameters," *Metallurgical Research & Technology*, 114, 614, http://dx.doi.org/10.1051/metal/2017073

Karalis K, Karkalos N, Cheimarios N, Antipas G, Xenidis A, Boudouvis AJ, 2016, "A CFD analysis of slag properties, electrode shape and immersion depth effects on electric submerged arc furnace heating in ferronickel processing," *Applied Mathematical Modelling*, 40, 9052-66, http://dx.doi.org/10.1016/j.apm.2016.05.045

Karimi-Sibaki E, Kharicha A, Wu M, Ludwig A, Bohacek J, Holzgruber H, et al, 2018, "A multiphysics model of the electroslag rapid remelting (ESRR) process," *Applied Thermal Engineering*, 130, 1062-9, http://dx.doi.org/10.1016/j.applthermaleng.2017.11.100

Kelkar KM, Patankar SV, Srivatsa SK, Minisandram RS, Evans DG, deBarbadillo JJ, et al, 2013, "Computational modeling of electroslag remelting (ESR) process used for the production of high-performance alloys," *Proceedings of the 2013 International Symposium on Liquid Metal Processing & Casting: Springer*, 3-12, http://dx.doi.org/%20978-3-319-48587-4

Li W-M, Jiang Z-H, Zang X-M, Deng X, 2017, "Modeling of flow and temperature distribution in electroslag remelting withdrawal process for fabricating large-scale slab ingots," *Journal of Iron and Steel Research International*, 24, 569-78, http://dx.doi.org/10.1016/S1006-706X(17)30087-0

Li X, Jiang Z, Geng X, Liu F, Peng L, Shi S, 2018, "Numerical simulation of a new electroslag remelting technology with current conductive stationary mold," *Applied Thermal Engineering*, 147， 736-46, http://dx.doi.org/10.1016/j.applthermaleng.2018.10.086

Liu F-B, Li Y-W, Jiang Z-H, Li H-B, Geng X, Chen X, 2015, "Electromagnetic behavior in electroslag remelting on laboratory scale and industrial scale," *Journal of central south university: natural science*, 46(10), 3580-85, http://dx.doi.org/10.11817/j.issn.1672-7207.2015.10.004

Miao Z-Q, Cheng G-G, Li S-J, Chen L, Liu Z-Q. Li C-W, 2018, "Mathematical model of electrode immersing depth in industrial electroslag remelting process and application," *Iron and Steel*, 53(09), 25-9, http://dx.doi.org/CNKI:SUN:GANT.0.2018-09-006

Ren N, Wang Q, Li B K, Li G Q, 2017, "Analysis of magnetic fluid flow and heat transfer in a three-phase electrode electroslag remelting system," *Large Casting forgings* (02), 13-16+24, http://dx.doi.org/10.14147/j.cnki.51-1396/tg.2017.02.005

Ren N, Li B, Li L, Qi F, Liu Z, 2018, "Numerical investigation on the fluid flow and heat transfer in electroslag remelting furnace with triple-electrode," *Ironmaking & Steelmaking*. 45, 125-34, http://dx.doi.org/10.1080/03019233.2016.1246847

Tong, W. J. , Li, W. M. , Zang, X. M. , Wang, P. , & Li, D. J., (2020), "Two-dimensional comprehensive mathematical model for electroslag remelting process with pipe electrode," *Journal of Iron and Steel Research International*., http:/dx.doi.org/10.1007/s42243-020-00426-9

Wang F, Li B-K, 2011, "Study on electromagnetic field and Joule Thermal Field of two-stage tandem electroslag remelting system," *Journal of Northeastern University: Natural Science*, 32(04), 80-3, http://dx.doi.org/10.3724/SP.J.1077.2010.10636

Wang Q, Zhao R, Fafard M, Li B-K, 2015, "Three-dimensional magnetohydrodynamic two-phase flow and heat transfer analysis in electroslag remelting process," *Applied Thermal Engineering*, 80, 178-86, http://dx.doi.org/10.1016/j.applthermaleng.2014.12.075

Wang Q, Cai H, Pan L, He Z, Liu S, Li B-K, 2016, "Numerical Investigation of Influence of Electrode Immersion Depth on Heat Transfer and Fluid Flow in Electroslag Remelting Process," *The Journal of Minerals, Metals & Materials Society*, 68, 3143-9, http://dx.doi.org/10.1007/s11837-016-2021-z

Wang Q, Wang F, Li G, Gao Y, Li B-K, 2017, "Simulation and experimental studies of effect of current on oxygen transfer in electroslag remelting process," *International Journal of Heat and Mass Transfer*, 113, 1021-30, http://dx.doi.org/10.1016/j.ijheatmasstransfer.2017.06.007

Wang X, Li Y, 2015, "A comprehensive 3D mathematical model of the electroslag remelting process," *Metallurgical and Materials Transactions B*, 46, 1837-49, http://dx.doi.org/10.1007/s11663-015-0342-x

Wang Z-X, Li Q, Wang L, 2018, "Engineering. Numerical Simulation of the Influence of Electrode Shrinkage Cavity on ESR Process of IN718 Alloy," *Rare Metal Materials and Engineering*, 47, 3579-89, http://dx.doi.org/10.1016/S1875-5372(19)30002-5

Yu J, Liu F-B, Jiang Z-H, Chen K, 2017, "Numerical Simulation of Electromagnetic Field of Industrial Scale Electroslag Remelting Process," *Journal of Northeastern University: Natural Science*, 38(5), 655-60, http://dx.doi.org/10.3969/j.issn.1005-3026.2017.05.010

Zhang S, Fan X. 2020, "Research on building glazed tile of fly ash added by radiation heat treatment inside catalytic combustion furnace of natural gas", *Frontiers in Heat and Mass Transfer*, 14, 9, http://dx.doi.org/10.5098/hmt.14.9